Cell Death and Differentiation (2016) 23, 358–368

www.nature.com/cdd

BAX inhibitor-1 is a Ca^{2+} channel critically important for immune cell function and survival

D Lisak[1], T Schacht[1], A Gawlitza[1], P Albrecht[2], O Aktas[2], B Koop[2], M Gliem[2], HH Hofstetter[2], K Zanger[3], G Bultynck[4], JB Parys[4], H De Smedt[4], T Kindler[5], P Adams-Quack[6], M Hahn[6], A Waisman[6], JC Reed[7], N Hövelmeyer[6] and A Methner*[,1]

The endoplasmic reticulum (ER) serves as the major intracellular Ca^{2+} store and has a role in the synthesis and folding of proteins. BAX (BCL2-associated X protein) inhibitor-1 (BI-1) is a Ca^{2+} leak channel also implicated in the response against protein misfolding, thereby connecting the Ca^{2+} store and protein-folding functions of the ER. We found that BI-1-deficient mice suffer from leukopenia and erythrocytosis, have an increased number of splenic marginal zone B cells and higher abundance and nuclear translocation of NF-κB (nuclear factor-κ light-chain enhancer of activated B cells) proteins, correlating with increased cytosolic and ER Ca^{2+} levels. When put into culture, purified knockout T cells and even more so B cells die spontaneously. This is preceded by increased activity of the mitochondrial initiator caspase-9 and correlated with a significant surge in mitochondrial Ca^{2+} levels, suggesting an exhausted mitochondrial Ca^{2+} buffer capacity as the underlying cause for cell death *in vitro*. *In vivo*, T-cell-dependent experimental autoimmune encephalomyelitis and B-cell-dependent antibody production are attenuated, corroborating the *ex vivo* results. These results suggest that BI-1 has a major role in the functioning of the adaptive immune system by regulating intracellular Ca^{2+} homeostasis in lymphocytes.

Cell Death and Differentiation (2016) **23,** 358–368; doi:10.1038/cdd.2015.115; published online 16 October 2015

The endoplasmic reticulum (ER) serves as the major intracellular calcium (Ca^{2+}) store, the release of which controls a vast array of cellular functions from short-term responses such as contraction and secretion to long-term regulation of cell growth and proliferation.[1] Dysregulated release of ER Ca^{2+}, in contrast, initiates programmed cell death by several mechanisms including mitochondrial Ca^{2+} overload, depolarization, ATP loss and cytochrome *c* release.[2] Besides this, the ER also has a key role in the synthesis, folding and sorting of proteins destined for the secretory pathway. The deleterious consequences of an increase in unfolded proteins is called ER stress and can be antagonized by the unfolded protein response (UPR), a mechanism that coordinates a simultaneous increase in the ER folding capacity and a decrease in folding load. In the case of insufficient adaptation to ER stress, cells undergo apoptosis.[3]

BAX (BCL2-associated X protein) inhibitor-1 (BI-1) is an evolutionarily conserved protein that bridges both the Ca^{2+} homeostasis and UPR functions of the ER.[4] BI-1 was first identified in a screen for human proteins capable of inhibiting BAX-mediated cell death in yeast.[5] In mammalian cells, BI-1's antiapoptotic function is most pronounced in paradigms of ER stress[6] and involves changes in the amount of Ca^{2+} that can be released from intracellular stores.[6,7] BI-1 is a highly hydrophobic protein that forms a Ca^{2+} pore responsible for its Ca^{2+} leak properties[8] and is the founding member of a family of six proteins with similar properties.[9] The increase in the ER Ca^{2+} leak mediated by BI-1 is blocked at a more acidic pH[10] – a function recently corroborated by a structural analysis of a bacterial homolog of BI-1.[11]

Despite its evolutionarily conserved role in important functions such as ER stress and Ca^{2+} regulation, *bi-1* –/– mice were reported to have no phenotypic abnormalities but increased infarct volumes in a stroke model, and increased sensitivity to tunicamycin-induced kidney toxicity.[6] Moreover, livers from BI-1-deficient mice regenerate faster than those from wild-type (WT) mice and this correlates with increased nuclear translocation of nuclear factor of activated T cells (NFATs)[12], a Ca^{2+}-dependent process. BI-1 knockout (KO) mice also express more of the spliced form of X-box-binding protein-1 (sXBP-1) in their liver and kidney,[13] which is generated by the endoribonuclease activity of inositol

[1]Focus Program Translational Neuroscience (FTN), Rhine Main Neuroscience Network (rmn^2) and Department of Neurology, University Medical Center of the Johannes Gutenberg University Mainz, Mainz, Germany; [2]Heinrich Heine Universität Düsseldorf, Department of Neurology, Düsseldorf, Germany; [3]Center for Anatomy and Brain Research, Düsseldorf, Germany; [4]Laboratory of Molecular and Cellular Signaling, Department of Cellular and Molecular Medicine, KU Leuven, Belgium; [5]III Medical Clinic, University Medical Center of the Johannes Gutenberg-University of Mainz, Mainz, Germany; [6]Institute for Molecular Medicine, University Medical Center of the Johannes Gutenberg-University of Mainz, Mainz, Germany and [7]Sanford Burnham Institute, La Jolla, CA, USA

*Corresponding author: A Methner, Focus Program Translational Neuroscience (FTN), Rhine Main Neuroscience Network (rmn^2) and Department of Neurology, University Medical Center of the Johannes Gutenberg University Mainz, Langenbeckstrasse 1, Mainz 55131, Germany. Tel: +49 6131 17 2695; Fax: +49 6131 17 5967; E-mail: axel.methner@gmail.com

Abbreviations: BAK, Bcl-2 homologous antagonist/killer; BAX, BCL2-associated X protein; BI-1, Bax inhibitor-1; EAE, experimental autoimmune encephalomyelitis; ER, endoplasmic reticulum; FACS, fluorescence-activated cell sorting; FCCP, carbonyl cyanide 4-(trifluoromethoxy) phenylhydrazoneFO, follicular; Grp78/BiP, glucose-regulated protein 78 kDa/binding immunoglobulin protein; IP_3, inositol 1,4,5-trisphosphate; IRE1, inositol requiring enzyme 1; KO, knockout; MZ, marginal zone; NADH, nicotinamide adenine dinucleotide hydride; NFAT, nuclear factor of activated T cell; NF-κB, nuclear factor-κ light-chain enhancer of activated B cells; NPCG, 4-hydroxy-3-nitrophenylacetyl coupled to chicken globulin; ROX, residual oxygen consumption; SERCA, sarcoplasmic/endoplasmic reticulum Ca^{2+}-ATPase; SOCE, store-operated Ca^{2+} entry; STIM1, stromal interaction molecule 1; UPR, unfolded protein response; WT, wild type; XBP-1, X-box-binding protein-1

Received 07.11.2014; revised 20.7.2015; accepted 21.7.2015; Edited by C Borner; published online 16.10.15

requiring enzyme 1 (IRE1), and is considered an indicator of increased UPR activity. This was later reproduced and attributed to an inhibitory function of BI-1 on IRE1α mediated via a direct interaction of the two proteins.[14]

In our study, we found that *bi-1−/−* mice are more obese and suffer from leukopenia. T and B cells from these mice show significant changes in cellular Ca^{2+} homeostasis and dynamics, and are more prone to spontaneous death in culture but, surprisingly, demonstrate no signs of ongoing ER stress within the homeostatic system of the living animal. These changes lead to an attenuated functioning of the adaptive immune system *in vivo*. Our results suggest that a major role of BI-1 *in vivo* involves its effects on the intracellular Ca^{2+} homeostasis in lymphocytes in line with its function as an ER Ca^{2+} leak channel.

Results

BI-1 mice are obese and suffer from leukopenia and erythrocytosis. Previously described BI-1 KO mice[6] were backcrossed to WT C57/BL6 mice and identified by genotyping because of the lack of functional antibodies.[15] A thorough phenotypic analysis of WT and KO littermates revealed that BI-1 KO mice at the age of 3 months are significantly more obese, even on a normal chow diet, and suffer from leukopenia (shown to be mainly lymphopenia and neutropenia by manual inspection) and erythrocytosis (Table 1). The effect of BI-1 deficiency therefore appears to be most pronounced with respect to homeostasis of the hematolymphoid system and energy balance.

BI-1 deficiency causes significant alterations of the B-cell compartment in the spleen. We focused on the immune system and studied the secondary lymphoid organs. The spleen, thymus, Peyers' patches and lymph nodes showed no gross abnormalities and were of similar size. The bone marrow, thymus, the peritoneal cavity and the spleen contained similar counts of total cells (Supplementary Figure 1a), and the subcellular composition of cells in the bone marrow (pro/pre, immature and mature recirculating B cells) and the thymus (CD4 and CD8 T cells) determined by flow cytometry were comparable (Supplementary Figures 1b–d). We also observed no significant difference in the percentage as well as total cell counts of splenic B and T cells of BI-1 KO mice compared with age-matched controls (Figure 1a).

Immature B cells leave the bone marrow and migrate to the spleen where they complete their maturation process. In the spleen, these cells become follicular (FO) B cells, which recirculate in the periphery, or marginal zone (MZ) B cells, which are largely sessile. An analysis of these cell types, immature ($CD21^{-}IgM^{-}$), FO ($CD21^{int}IgM^{high}$) and MZ ($CD21^{high}IgM^{neg\text{-}low}$) B cells revealed a significant elevation of MZ B cells in KO spleens (KO $20.5 \pm 5.2\%$ *versus* WT $10.9 \pm 2.7\%$) at the expense of FO B cells (Figure 1b). This was also evident in splenic sections stained with an anti-CD1d antibody, which recognizes MZ B cells. Interestingly, in the KO mice, MZ B cells were also found within the follicles, whereas in controls, strong CD1d staining was only detected in the MZ as expected (Figure 1c). Taken together, these results demonstrate a significant increase in the generation, differentiation or maintenance of mature MZ cells at the expense of FO B cells in BI-1 KO mice compared with WT controls.

Increased constitutive nuclear translocation of the transcription factor NF-κB in BI-1 KO splenocytes. Such a shift towards MZ B cells has been previously linked to NF-κB (nuclear factor-κ light-chain enhancer of activated B cells) signaling. NF-κB1 (p105/p50) and NF-κB2 (p100/p52) need to be processed to become active and translocate to the nucleus where they associate with RelA (p65), c-Rel and RelB in different hetero- and homodimers to form the transcriptionally active complex.[16] Mice deficient in RelB show reduced numbers of MZ B cells,[17] whereas mice lacking a negative regulator of NF-κB have more MZ B cells[18] similar to mice that lack the inhibitory p100 subunit of NF-κB2.[19]

We therefore quantified the abundance of all NF-κB proteins in the cytosol and the nucleus by immunoblotting of subcellular fractions obtained from freshly isolated splenocytes. This revealed an increased cytosolic abundance of c-Rel and RelA and an increased nuclear abundance of RelB in BI-1 KO cells (Figure 2a), whereas the proteins that lack transcriptional activation domains, NF-κB1/2, remained unchanged (Supplementary Figure 2a). Because of the feeble nuclear abundance of RelA (p65) in these unstimulated cells, we used immunocytochemistry with another antibody and quantification by high-content imaging as an additional read-out. In these experiments, RelA (p65) translocated to the nucleus to a much higher degree ($P<0.0001$) in BI-1-deficient splenocytes, as suggested by the immunoblotting experiments (Figure 2b).

Table 1 Body weight and laboratory results from WT and KO mice

	WT	KO	*P*-value
Body weight (g ± S.D.)	23.1 ± 1.821	26.2 ± 2.186	0.0235
Leukocytes (x10E3/μl ± S.D.)	3.73 ± 0.95	1.94 ± 1.14	0.0043
Erythrocytes (x10E6/μl ± S.D.)	9.10 ± 1.08	10.38 ± 0.79	0.0403
Thrombocytes (x10E3/μl ± S.D.)	530.00 ± 144.24	520.50 ± 182.47	0.9097
Hematocrit (% ± S.D.)	47.32 ± 5.25	52.78 ± 2.56	0.0454
Mean corpuscular volume (fl ± S.D.)	52.03 ± 0.92	50.5 ± 1.91	0.1073
Mean corpuscular hemoglobin (pg ± S.D.)	15.45 ± 0.26	14.88 ± 0.30	0.0057
Mean corpuscular hemoglobin (gxHb/dl ± S.D.)	29.67 ± 0.37	29.50 ± 0.96	0.6993
Alanine transaminase (U/l ± S.D.)	23.4 ± 5.90	19.83 ± 8.47	0.4488
Aspartate transaminase (U/l ± S.D.)	67.20 ± 19.29	84.83 ± 44.41	0.4334

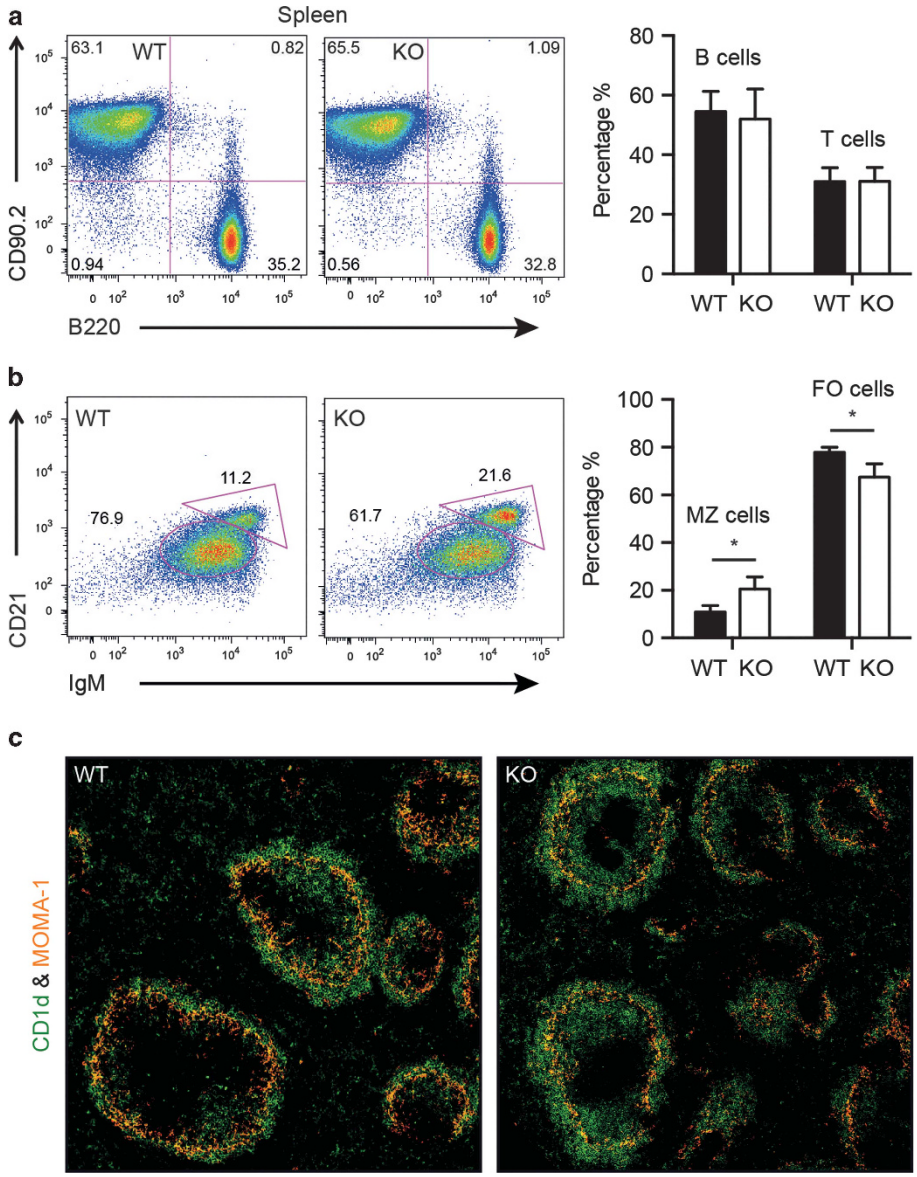

Figure 1 BI-1 deficiency causes significant alterations of the B-cell compartment. Flow cytometric analysis of splenic cells from 8- to 12-week old WT and BI-1 KO mice. T and B cells were stained with (**a**) B220 and CD90.2 antibodies, and (**b**) MZ and FO B cells with IgM and CD21 antibodies pregated on live B220$^+$ B cells. Bar graphs show the mean $\pm$ S.E.M., $n=3$. Data were analyzed by two-tailed *t*-tests, $^*P<0.05$. (**c**) Representative immunofluorescence analysis of MZ B cells stained with α-CD1d and metallophillic macrophages stained with α-MOMA-1 in spleen tissue sections

In unstimulated cells, the Rel/NF-κB dimers associate with members of the family of inhibitor proteins called IκBs and remain inactive in the cytoplasm. In NF-κB not bound by IκBα in the cytosol, the nuclear localization signal of p65 is liberated, which allows its translocation into the nucleus. The NF-κB/IκB ratio thus determines the amount of nuclear-translocated NF-κB and this ratio was indeed increased in BI-1 KO splenocytes (Figure 2c). IκB is usually removed from NF-κB by activation of the IκB kinase complex, which leads to phosphorylation of IκBα, resulting in ubiquitination and degradation of IκBα. Phosphorylated IκBα was downregulated in BI-1 KO splenocytes (Figure 2d). We conclude that NF-κB proteins harboring a transcriptional activation domain are upregulated and show an increased nuclear localization in the absence of BI-1, which may explain the increase in MZ B cells in these animals compared with controls.

BI-1 KO splenocytes have increased ER and cytosolic Ca^{2+} levels and a compensatory downregulation of store-operated Ca^{2+} entry. NF-κB is activated in a pleiotropic manner including changes in the amplitude and duration of Ca^{2+} signals in lymphocytes.[20,21] Also, treatment with inhibitors of sarcoplasmic/ER Ca^{2+}-ATPases (SERCA), which increase cytosolic Ca^{2+}, causes nuclear NF-κB translocation.[22] NF-κB can also be activated by a pathological mechanism known as the ER overload reaction. This condition is caused by retention of proteins within the ER lumen, and in contrast to the UPR does not induce Grp78/BiP

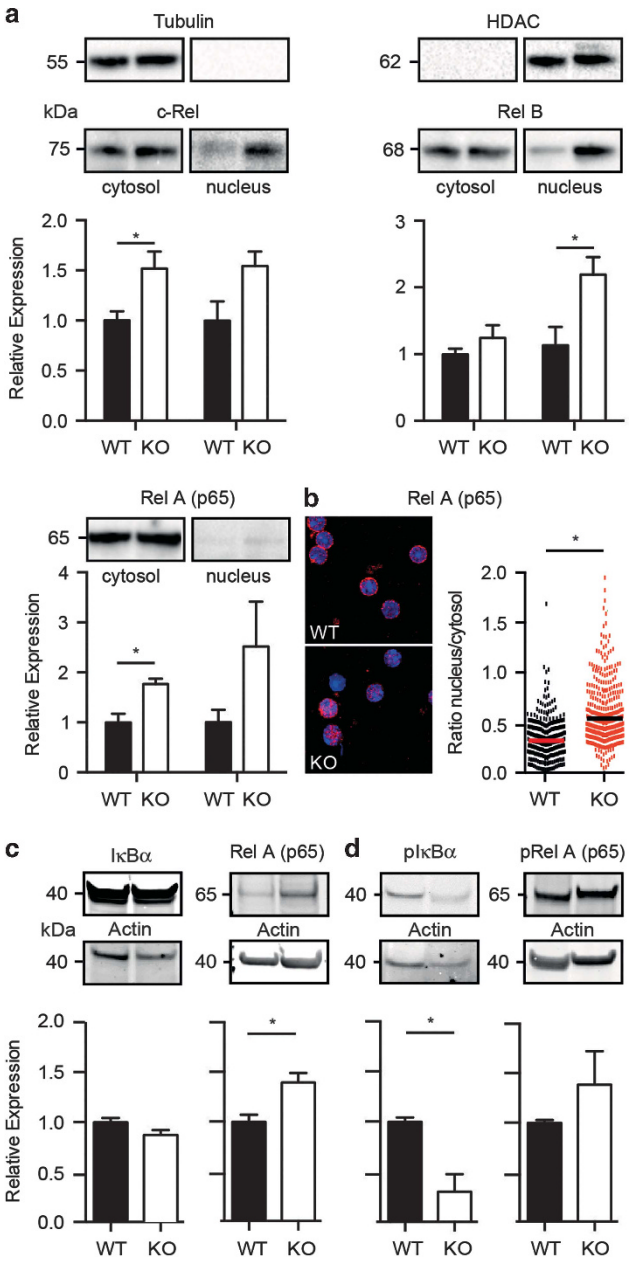

Figure 2 Increased expression and nuclear translocation of class II NF-κB proteins in BI-1 KO splenocytes. (**a**) Immunoblots with cytosolic and nuclear fractions obtained from WT and KO splenocytes incubated with antibodies against class II NF-κB proteins show increased cytosolic and nuclear abundance in BI-1 KO splenocytes. Loading controls, α/β-tubulin for the cytosolic fraction and HDAC for the nuclear fraction, are shown on the top. Molecular weight is indicated. Bar graphs show mean intensity values normalized to WT ± S.E.M., $n=8$. (**b**) Increased nuclear localization of RelA (p65) shown by quantitative immunocytochemistry in BI-1 KO splenocytes. Splenocytes were stained with an α-RelA (p65) antibody and analyzed by confocal microscopy. Quantification was carried out on a high-content imaging microscope by measuring the fluorescence intensity in the nucleus defined by DAPI (4',6-diamidino-2-phenylindole) staining and in the cytosol defined as an area around the nucleus. The scatter plot shows the ratio of nuclear to cytosolic RelA (p65) (300 WT and 432 KO cells, $n=3$ independent experiments, mean is indicated). (**c**) Increased ratio of RelA (p65) and IκBα and (**d**) downregulated phosphorylated IκBα in BI-1 KO splenocytes. Actin served as a loading control on the same blot, size is indicated. Bar graphs show mean intensity values normalized to WT ± S.E.M., $n=6$. Data were analyzed by two-tailed *t*-tests, $^*P<0.05$

(glucose-regulated protein 78 kDa/binding immunoglobulin protein),[23] which is also unchanged in the absence of BI-1.[12,13] Notably, NF-κB induction by the ER overload reaction can be attenuated by intracellular Ca^{2+} chelators.[24,25]

Therefore, both major functions of BI-1, its role in ER stress and in the maintenance of the intracellular Ca^{2+} homeostasis, might be implicated in the observed phenotype. We first investigated the relative abundance of UPR proteins by immunoblotting of splenocyte lysates from BI-1 KO and WT mice and detected no evidence of ongoing ER stress in BI-1-deficient splenocytes. Rather, several of the UPR proteins were downregulated, especially ERp57. Importantly, BiP was unchanged (Supplementary Figure 3a). Despite the role of BI-1 as a direct inhibitor of IRE1α,[14] we observed decreased XBP-1 splicing in KO cells (Supplementary Figure 3b) in line with the decreased expression of ER stress-regulated chaperones. We concluded that the UPR and the ER overload reactions are not constitutively active in splenocytes isolated directly from BI-1 KO mice.

The other major role of BI-1 is the regulation of cellular Ca^{2+} homeostasis. Using flow cytometry of freshly isolated splenocytes, we measured resting Ca^{2+} levels in WT and KO splenocytes with Fluo8-AM and found increased cytosolic Ca^{2+} levels in KO cells (Figure 3a). We next quantified the ER Ca^{2+} content and store-operated Ca^{2+} entry (SOCE) from the extracellular space, which is activated by a decrease in $[Ca^{2+}]_{ER}$ using the ratiometric probe Fura2. The cells were attached to plates to allow a kinetic analysis of (1) Ca^{2+} passively leaking from the ER after inhibition of the Ca^{2+} reuptake pump SERCA in the absence of extracellular Ca^{2+} and then (2) Ca^{2+} re-entry from SOCE after re-exposure of the cells to large amounts of extracellular Ca^{2+}. BI-1 KO splenocytes had an increased baseline Ca^{2+} concentration (corroborating the results obtained with Fluo8), an increased thapsigargin-releasable ER Ca^{2+} pool and reduced SOCE (Figure 3b).

This SOCE reduction is mediated by a downregulation of Orai1, the plasma membrane channel mediating SOCE,[26,27] and probably serves as a compensatory mechanism to limit filling of the already Ca^{2+}-full ER (Figure 3c). Taken together, these data corroborate that BI-1 deficiency causes profound alterations of the intracellular Ca^{2+} homeostasis in freshly isolated splenocytes, which manifests as increased Ca^{2+} concentrations in the ER, and, surprisingly, also in the cytoplasm. It is thus possible that the alterations in the intracellular Ca^{2+} homeostasis are implicated in the observed increase in NF-κB nuclear translocation.

To test this assumption, we investigated the cellular localization of another transcription factor, NFAT, which translocates to the nucleus upon the pronounced Ca^{2+} release from the ER in response to activation of the antigen receptors.[21] We observed that NFATc1 was also already translocated to a much higher degree in BI-1-deficient splenocytes even without stimulation, similar to NF-κB (Figure 3d) but unchanged at the expression level (Figure 3e). These data corroborate results obtained in BI-1-deficient hepatocytes, which also showed an increased constitutive translocation of NFATc1,[12] and support the assumption that the changes in Ca^{2+} signaling are responsible for the increased abundance and nuclear translocation

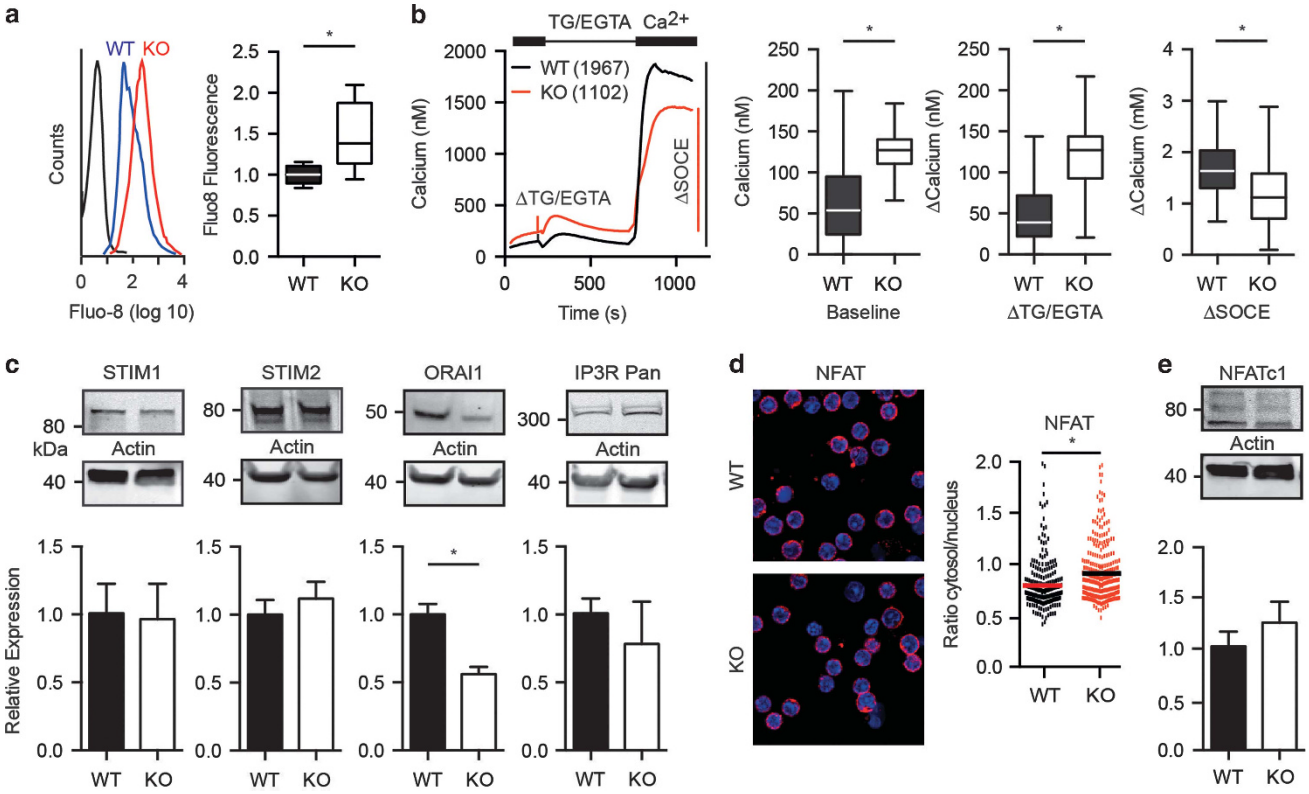

Figure 3 Increased ER and cytosolic Ca^{2+} levels cause increased constitutive nuclear translocation of the Ca^{2+}-dependent transcription factor NFAT in BI-1 KO splenocytes. (**a**) Increased cytosolic Ca^{2+} in BI-1 KO splenocytes measured by flow cytometry of splenocytes stained with Fluo8-AM. Fluo8-AM fluorescence at 488 nm is proportional to the amount of bound Ca^{2+} and is quantified as mean fluorescence intensity (MFI). The histogram shows representative data of unstained (black), WT (blue) and BI-1 KO (red) splenocytes where each cell is plotted against its relative fluorescence intensity on a log scale. Box and whiskers show the quantification of data normalized to WT animals ($n=12$, median, box from the 25th quartile to the 75th quartile, whiskers minimum to maximum). (**b**) BI-1 KO splenocytes have increased baseline Ca^{2+} and an increased thapsigargin-releasable Ca^{2+} pool but decreased store-operated Ca^{2+} entry (SOCE). Cells stained with Fura2-AM were attached to poly-L-lysine-coated plates and the intracellular Ca^{2+} concentration recorded in response to the indicated SOCE protocol on a high-content imaging microscope. The traces show the mean of the calibrated Ca^{2+} concentration from three pooled independent experiments. The box and whisker plot represent the statistical distribution of the absolute Ca^{2+} concentration at baseline, the baseline-corrected thapsigargin-releasable pool and the amount of Ca^{2+} that entered the cell during SOCE. (**c**) Orai1 is downregulated in BI-1 KO splenocytes. Immunoblots were incubated with α-STIM1, α-STIM2, α-ORAI1 and α-pan IP_3R antibodies. Actin served as a loading control on the same blot; size is indicated. Bar graphs show mean intensity values normalized to WT $\pm$ S.E.M., $n=6$. (**d**) Increased nuclear localization of NFATc1 in BI-1 KO splenocytes. Splenocytes were stained with α-NFATc1 and analyzed by confocal microscopy. Quantification was carried out on a high-content imaging microscope by measuring the fluorescence intensity in the nucleus defined by DAPI (4',6-diamidino-2-phenylindole) staining and in the cytosol defined as an area around the nucleus. The scatter plot shows the ratio of nuclear-to-cytosolic NFAT (275 WT and 312 KO cells from $n=3$ independent experiments. The mean is indicated. (**e**) The expression of all three NFATc1 isoforms is not regulated in BI-1 KO splenocytes. Immunoblots were incubated with an α-NFATc1 antibody. Actin served as a loading control on the same blot; size is indicated. Bar graphs show mean intensity values normalized to WT $\pm$ S.E.M., $n=6$. Data were analyzed by two-tailed *t*-tests, $^*P<0.05$

of NF-κB in BI-1-deficient lymphocytes and thus for the changes in MZ cell abundance.

We next investigated alterations of the Ca^{2+} homeostasis and NF-κB translocation in purified T and B cells. Fluo8-AM staining revealed higher resting cytosolic Ca^{2+} concentrations in B cells compared with T cells (Figure 4a) matching nuclear translocation levels of RelA (p65) (Figure 4b). To study physiological ligand-activated Ca^{2+} release, we incubated Fluo8-stained splenocytes with biotinylated anti-CD3 antibodies and measured Fluo8 intensity by flow cytometry for 60 s to establish a baseline. Then, streptavidin was added to crosslink the anti-CD3 antibodies on the surface, which activates the T-cell receptor and elicits inositol 1,4,5-trisphosphate (IP_3)-dependent Ca^{2+} release from the ER and subsequent SOCE. B cells were similarly stimulated by the addition of anti-IgM. Both KO T and B cells showed increased baseline Ca^{2+} concentrations and B cells also showed an increased Ca^{2+} release after stimulation (Figure 4c). To further substantiate this, we then quantified IgM-mediated increases in the mitochondrial electron transfer capacity of B cells from WT and KO animals. IgM-mediated Ca^{2+} release from the ER elevates mitochondrial matrix [Ca^{2+}], thereby stimulating Krebs' cycle dehydrogenases and elevating mitochondrial [NADH],[28] which is then fed into the oxidative phosphorylation pathway. This indeed revealed an increased stimulation in KO cells as a functional readout of the increased ER Ca^{2+} release (Figure 4d).

Increased spontaneous B-cell death in culture is associated with exhausted mitochondrial Ca^{2+} buffering capacity and caspase activation. When we took purified T and B cells into culture, we noted that after 24 h, KO cells were much more prone to spontaneous cell death. This was again more pronounced in B cells (Figure 5a) and we focused

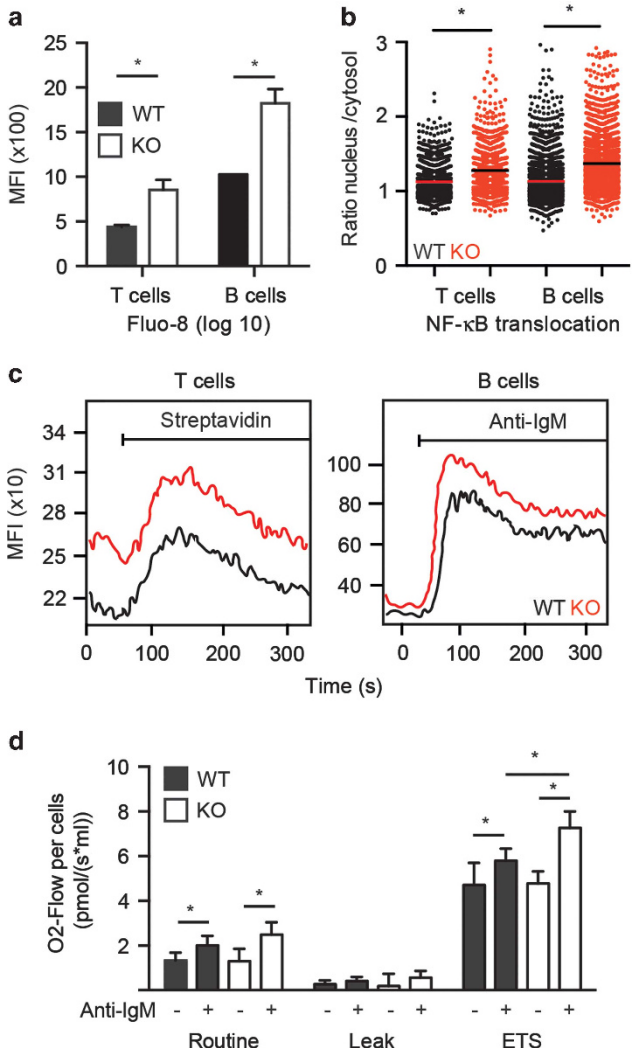

Figure 4 T and B cells are affected by BI-1 deficiency. (**a**) Basal cytosolic Ca^{2+} is increased in BI-1 KO T and B cells. Magnetically sorted and negatively selected T and B cells were incubated with Fluo8-AM and the fluorescence measured by flow cytometry. Bar graphs represent the average mean fluorescence intensity as the median ± S.D., $n=6$. (**b**) Increased RelA (p65) nuclear localization in BI-1 KO B and T cells. B and T cells were magnetically sorted and negatively selected and stained with an RelA (p65) antibody and DAPI (4',6-diamidino-2-phenylindole). Quantification was carried out on a high-content imaging microscope by measuring the fluorescence intensity in the nucleus defined by DAPI staining and in the cytosol defined as the area around the nucleus. The scatter plot shows the ratio of nuclear to cytosolic RelA (p65) (B cells: 1931 WT and 1968 KO cells; T cells: 971 WT and 941 KO cells) from three independent experiments. The mean is indicated. Data were analyzed by two-tailed *t*-tests, $^*P<0.05$. (**c**) Ligand-induced Ca^{2+} release in BI-1 KO T and B cells quantified by flow cytometry. Fluo8-AM fluorescence at 488 nm is proportional to the amount of bound Ca^{2+} and is quantified as mean fluorescence intensity (MFI). Splenocytes were incubated with biotinylated anti-CD3 antibody and stimulated with streptavidin or directly stimulated with anti-IgM after 60 s of baseline. Streptavidin causes the biotinylated anti-CD3 to cluster and thereby activates T cells, whereas anti-IgM selectively activates B cells. Representative traces of Fluo8 kinetics are shown for WT (black) and BI-1 KO (red) T and B cells. (**d**) Increased electron transfer system (ETS) capacity in BI-1 KO B cells treated with anti-IgM measured by high-resolution respirometry. Routine respiration was measured under basal conditions, leak respiration after inhibition of ATP synthase using oligomycin and the ETS capacity at maximum uncoupling with FCCP and oxygen flow. All measurements were corrected for residual oxygen consumption after inhibition of complex I with rotenone and complex III with antimycin A. Shown is the mean ± S.D., $n=4$ mice. Data were analyzed by two-tailed *t*-tests, $^*P<0.05$

on these cells for further investigations of the impact of BI-1 deficiency. An analysis by electron microscopy of purified B cells revealed alterations in the texture of the cytoplasm, defective organelles (e.g., mitochondria) and the presence of nuclear inclusions in nearly all KO cells (Supplementary Figure 4). Quantification of B-cell death in a time-course analysis by flow cytometry revealed a statistically significant difference in viability after only 4 h in culture (WT 11.0 ± 1.2% and KO 15.6 ± 0.3%) that increased over time. After 24 h in culture, >68 ± 4.8% of KO cells were dead compared with 28 ± 5.9% WT cells (Figure 5b).

Because caspases are principal effectors of apoptosis, we measured the activity of the effector caspases 3 and 7 after placing B cells into culture. We detected a significant difference between KO and WT cells already after 4 h in culture, with higher relative levels of effector caspase activity in the KO cells (Figure 5c). We quantified the activity of initiator caspases 8 and 9, which represent the apical proteases in the 'extrinsic' and 'intrinsic' apoptosis pathways, respectively, after 3 h in culture (thus before effector caspase activation became different). Activity of both of these initiator caspases was significantly higher in BI-1 KO compared with WT B cells (Figure 5d), with relative levels of caspase-9 activity considerably higher compared with caspase-8 in both KO and WT B cells placed into culture.

Caspase-9 activation classically involves cytochrome *c* release from the mitochondria,[29] which can be stimulated by a Ca^{2+}-dependent mechanism that impacts inner membrane permeability, followed later by rupture of the outer membrane.[2] BI-1 is capable of regulating Ca^{2+} transport between ER and mitochondria,[30] leading us to hypothesize that the altered ER and cytoplasmic Ca^{2+} levels in BI-1-deficient cells might be reflected by similar alterations of mitochondria. Measuring mitochondrial [Ca^{2+}] using Rhod2-AM in freshly isolated B cells from KO *versus* WT animals demonstrated that Rhod2-AM fluorescence was only slightly increased at baseline but much more significantly after 4 h in culture (Figure 5e), whereas the difference between KO and WT in cytosolic [Ca^{2+}] declined (Figure 5f). Levels of reactive oxygen species (Figure 5g) and XBP-1 splicing (Figure 5h), in contrast, did not differ in WT and KO cells at baseline or after 4 h. Exposure of these cells to different pH or extracellular [Ca^{2+}] did not profoundly affect cell death or cytosolic and mitochondrial Ca^{2+} levels (Figure 5i).

These data suggest that mitochondria of BI-1-deficient B cells exceed their buffering capacity after a few hours in culture, and we envisaged that clamping the intracellular Ca^{2+} with the cell-permeable Ca^{2+} buffer BAPTA-AM should inhibit this Ca^{2+}-dependent cell death. However, this experimental approach was not possible because BAPTA-AM treatment rapidly killed primary B cells (not shown), as has previously been shown for leukemic cells.[31] Thus, the observed defects in mitochondrial Ca^{2+} buffering capacity seen in cultured BI-1 KO B cells are correlated with caspase activation and cell death, but a direct cause and effect relationship was not demonstrable.

BI-1 deficiency attenuates T- and B-cell function *in vivo*. We finally aimed to clarify the effect of the identified changes in T and B cells on immune system function *in vivo*

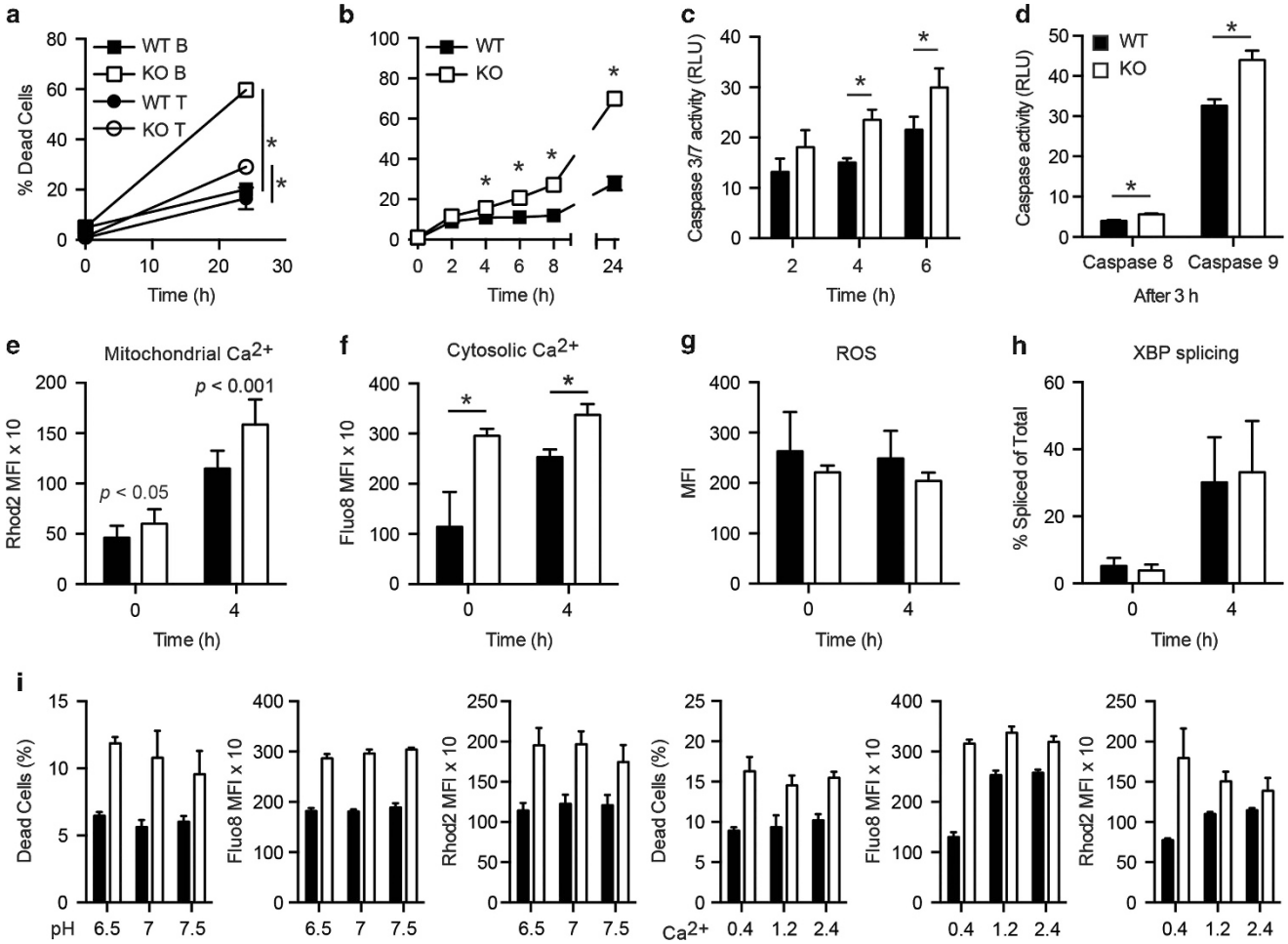

Figure 5 Increased spontaneous B-cell death in culture is caused by an exhausted mitochondrial Ca^{2+} buffer capacity leading to caspase activation. (**a**) B and T cells were magnetically sorted, negatively selected and put into culture. Cell death was assessed 24 h later by flow cytometry using a live/dead stain and demonstrates increased spontaneous cell death in KO splenocytes with B cells being more susceptible compared with T cells. (**b**) A time-course analysis of B-cell death with significant differences already evident after 4 h in culture. Cell death was assessed as described in (**a**). The graphs in (**a** and **b**) show the mean percentage of dead cells ± S.E.M. from six mice at each time point. (**c**) Caspase-3/7 activity in both WT and BI-1 KO B cells increases in a time-dependent manner and becomes significantly increased in KO cells at 4 h in culture. (**d**) Caspase-8 and -9 are significantly increased in BI-1 KO B cells after 3 h in culture, with caspase-9 being more prominent. All caspase activity was assessed in magnetically sorted and negatively selected B cells using a luminescent caspase assay. Caspase-8 and -9 were assessed in parallel. Bar graphs represent the mean average relative luminescence ± S.E.M. from six mice measured in triplicates (**e**–**g**) After 4 h in culture, the mitochondrial Ca^{2+} is significantly increased in KO B cells. Magnetically sorted and negatively selected B cells were stained with (**e**) Rhod2-AM, (**f**) Fluo8-AM or (**g**) CellROX at the indicated time points. The graph represents the mean fluorescence intensity ± S.D., $n = 3$–6. Data were analyzed by two-tailed *t*-tests, $^*P < 0.05$. (**h**) XBP-1 splicing was assessed by PCR in magnetically sorted and negatively selected B cells at the indicated time points in culture. Bar graphs show the mean percentage ± S.D. of spliced XBP-1/(spliced XBP-1+unspliced XBP-1) from six mice. Data were analyzed by two-tailed *t*-tests, $^*P < 0.05$. (**i**) Magnetically sorted and negatively selected B cells were stained with a live/dead stain, Fluo8-AM or Rhod2-AM after 4 h in culture. In the pH experiments, the cells were cultured as normally and put into HBSS buffer with the indicated pH immediately after staining and directly processed; in the Ca^{2+} experiments, the culturing medium was adjusted with $CaCl_2$ (mM) and EGTA and processed as described above. Bar graphs represent the mean fluorescence intensity as the median ± S.D., $n = 6$–24 mice

using two different experimental paradigms. First, in experimental autoimmune encephalitis (EAE), the immune system is challenged by immunization with myelin proteins emulsified in complete Freund's adjuvant, causing a mainly T-cell-driven autoimmunity against the central nervous system and the development of a multiple sclerosis-like disease that can be scored for severity. KO mice displayed a later onset of clinical symptoms and an overall lower clinical score (Figure 6a), despite the fact that the brain of BI-1 KO mice appears to be more vulnerable to exogenous stress, as shown by larger infarcts in a stroke model.[6] The attenuated EAE disease score was associated with reduced infiltration of microglia as well as a decreased number of lesions detectable by immunohistochemistry (Figures 6b and c). Second, to assess B-cell function, we immunized the mice with 4-hydroxy-3-nitrophenylacetyl coupled to chicken globulin (NPCG), which is a standard T-cell-independent immunogen,[32] and then quantified the resulting antibody response. BI-1 KO animals generated significantly lower amounts of IgG1 and IgG2b in response to this antigen (Figure 6d). We conclude that both T- and B-cell functions are attenuated *in vivo*, thereby corroborating the *in vitro* changes. To clarify whether this is because of defective cell signaling or the reduced number of lymphocytes *in vivo*, we investigated *in vitro* isotype switching of splenic B cells. In these experiments, splenocytes stimulated *ex vivo* with LPS and IL-4 start producing IgG1,

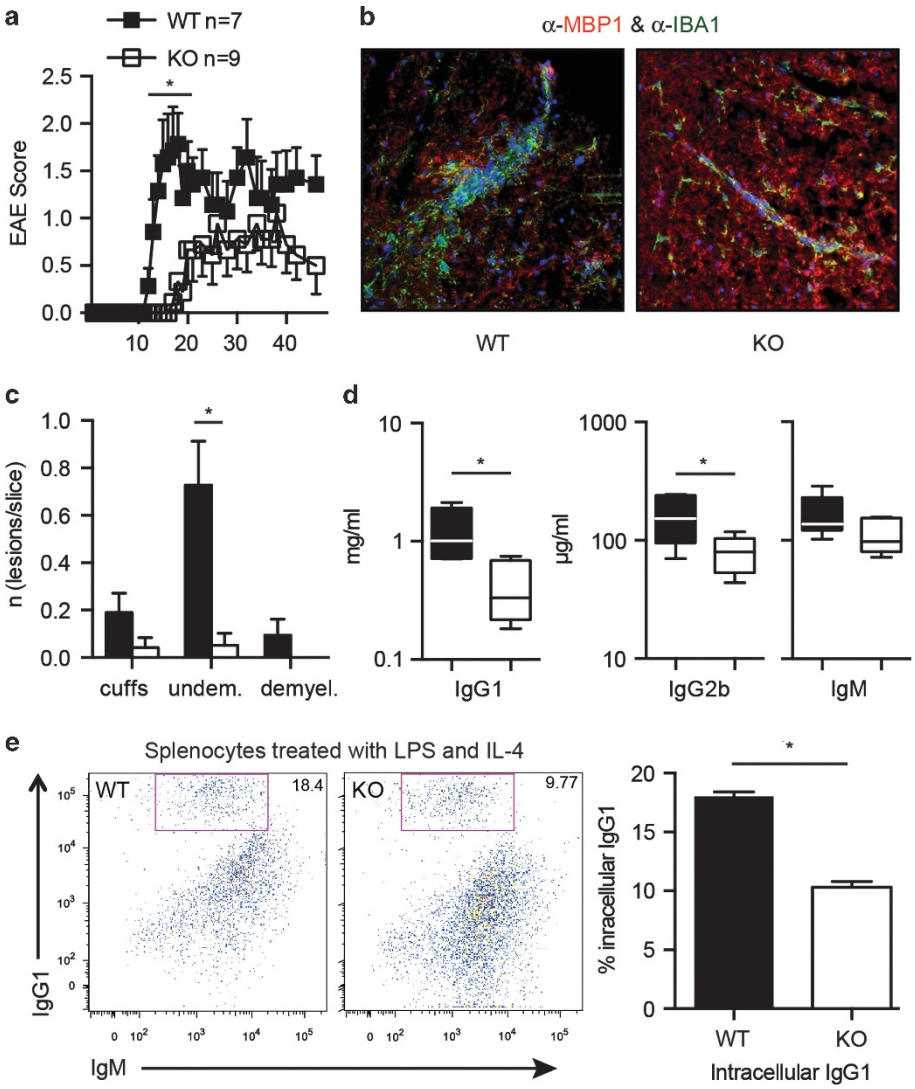

Figure 6 BI-1 deficiency attenuates T- and B-cell function. (**a**) BI-1 KO mice are less susceptible to EAE elicited by immunization with the $MOG_{35–55}$ peptide. Individual clinical disease scores (1, limp tail; 2, weakness of hind legs; 3, hind leg paralysis; 4, hind and front leg paralysis; 5, death) were assessed daily. Shown is the mean ± S.E.M. of the daily average score for the indicated number of WT and BI-1 KO mice from one representative experiment of three. (**b**) Histopathology of cryosectioned brain stained with Iba1 (microglia, green), MBP (myelin, red) and Hoechst (nuclei, blue) shows less demyelination in BI-1 KO mice. (**c**) Cuffs and lesions caused by intruding microglia were counted 15 days after immunization. Cuffs are inflammatory vessel-centered lesions without tissue infiltration, undemyelinated (undem) is defined as parenchymal lesions without demyelination and demyelinated (demyel) is defined as parenchymal lesions with demyelination. Three to eight sections from seven mice were quantified and BI-1 KO mice show a significantly reduced number of undemyelinated lesions per section (WT 0.7 ± 0.4 *versus* BI-1 KO 0.05 ± 0.09). Bar graphs show the average number of lesions per section of each genotype as the mean ± S.E.M. (**d**) Attenuated immunoglobulin production quantified by ELISA 10 days after immunization with NPCG precipitated in Alum in BI-1 KO mice. (**e**) Class switching of BI-1 KO and control splenocytes and CD19+ B cells at day 4 of *in vitro* stimulation with LPS+IL-4. IgG1 of 200 000 events was quantified by intracellular staining as indicated. Bar graphs show the mean ± S.E.M., $n = 3$. The box and whiskers represent the median amount of the indicated immunoglobulins with the box extending from the 25th quartile to the 75th quartile and the whiskers represent the minimum and maximum values ($n = 10$). EAE data were analyzed by two-way ANOVA with Bonferroni *post hoc* correction; all other data were analyzed by two-tailed *t*-tests, $^*P < 0.05$

which can be quantified intracellularly by flow cytometry. Upon this treatment, significantly less BI-1 KO cells switched to IgG1 compared with control splenocytes, suggesting that defective signaling is involved in the observed phenotype (Figure 6e).

Discussion

Our observations indicate that BI-1 has a major role in the correct functioning of the adaptive immune system. B and T cells malfunction apparently because of profound changes in intracellular Ca^{2+} homeostasis and dynamics. All aspects of the cellular Ca^{2+} machinery are altered in the absence of functioning BI-1 and this correlates with an enhanced nuclear translocation of Ca^{2+}-dependent transcription factors and an overload of the mitochondrial Ca^{2+} buffer capacity leading to spontaneous cell death in culture. These results are well in line with previously reported effects of BI-1 in the control of the ER Ca^{2+} content.[6–8,10] Also, structural evidence obtained from a bacterial homolog of BI-1 just demonstrated that BI-1 is indeed a Ca^{2+} leak channel with an evolutionarily conserved pH sensor.[11]

We observed an increased ER Ca^{2+} concentration as expected for cells lacking an important ER Ca^{2+} leak channel and a reduced SOCE caused by downregulation of the plasma membrane Ca^{2+} channel Orai1. It is clear that the already overfilled ER does not need further filling, but why and how does this result in the observed increase in cytosolic Ca^{2+} concentration?

In BI-1 KO, there is less Ca^{2+} leak from the ER, and, hence, more Ca^{2+} is available for IP_3-induced Ca^{2+} release, which can explain the higher Ca^{2+} transients. It is possible that even under resting conditions, constitutive activation of B- or T-cell receptors provokes basal Ca^{2+} release, which is expected to be higher in KO cells. Cytosolic Ca^{2+} transients are normally cleared efficiently by extrusion to the extracellular space or immediate refilling of the ER by SERCA, which (i) is apparently less effective in immune cells in general, thereby explaining why this phenotype is most pronounced in the immune system[33] and (ii) is directly inhibited by the Ca^{2+} load of the store.[34] It was also shown previously that a high ER Ca^{2+} load negatively regulates Ca^{2+} reuptake from the cytosol,[35] which is probably mediated by the oxidoreductase ERp57. In conditions of high luminal Ca^{2+}, like in the absence of functional BI-1, ERp57 binds SERCA2b (the ubiquitously expressed isoform) and inhibits its activity through the facilitation of disulfide bond formation in the longest ER facing loop of SERCA2b.[36] As we observed an unexpected downregulation of the UPR target protein ERp57 in BI-1 KO splenocytes, we speculate that this represents a compensatory mechanism to remove the breaks from SERCA2b and relieve the cell from the excessive cytosolic Ca^{2+} load.

Finally, how can we resolve our findings with the proposed function of BI-1 as a direct inhibitor of IRE1α?[14] IRE1α not only interacts with BI-1 but also with the proapoptotic proteins BAX and BAK (Bcl-2 homologous antagonist/killer), which in contrast to BI-1 activate IRE1α signaling.[37] Cells lacking both proteins have a reduced ER Ca^{2+} concentration[38] because of an increased Ca^{2+} leak[39] and therefore behave like BI-1-overexpressing cells.[7] As BI-1 does not directly interact with BAX/BAK[5,14] but attenuates the interaction of BAX with IRE1α,[14] it was speculated that BI-1 acts upstream of these proteins in the control of IRE1α inactivation.[14] However, maybe the proposed inactivation of IRE1α by BI-1 is reciprocal, meaning that IRE1α also inhibits BI-1 channel activity. To the best of our knowledge, this has not yet been studied. In this scenario, the lack of BAX/BAK in double KO cells would inhibit IRE1α, thereby activating BI-1 and causing a reduction in the ER Ca^{2+} concentration, which is in accordance with reported results.

In summary, our findings present *in vivo* evidence that the Ca^{2+} channel activity of BI-1 is critically important for immune cell function and survival.

Materials and Methods

Animals and laboratory tests. BI-1 KO mice first described by Chae *et al.*[6] were identified by genotyping according to the published protocol and backcrossed to WT C57/Bl6 mice for more than generations. All mice were maintained in the local animal facility. All animal experiments were fully approved by local authorities for animal experimentation. Mice were age and sex matched and 8–12 weeks old. The blood count and liver enzyme analysis were carried out by the clinical laboratory of the University Hospital Düsseldorf. A differential blood count was carried out manually in stained blood streaks.

Flow cytometry. Single-cell suspensions were prepared from different organs and the erythrocytes lysed with tris-ammonium chloride, pH 7.2. Cells were treated with Fc-block (Affymetrix eBioscience, San Diego, CA, USA), washed and surface stained with antibodies against CD5, CD19, CD21 (7G6), CD23, CD90.2, and IgD, B220 and anti-IgM (BD Bioscience, Franklin Lakes, NJ, USA). All samples were measured on a FACSCanto II (Becton, Dickinson, Franklin Lakes, NJ, USA) and analyzed with FlowJo, LLC (Ashland, OR, USA).

Immunohistochemistry. Animals were perfused and tissues fixed with 4% paraformaldehyde (Carl Roth, Karlsruhe, Germany). Thick slices (20 μM) of the spinal cord and 8 μm sections from spleens were cut in a cryotome (Leica Mikrosysteme Vertrieb GmbH, Wetzlar, Germany) and stained with primary antibodies against CD1d (Affymetrix eBioscience), MOMA-1 (Affymetrix eBioscience), Iba1 (Wako Chemicals GmbH, Neuss, Germany; 1 : 800) and MBP (EMD Millipore, Billerica, MA, USA; 1 : 500). Iba1 and MBP were detected with secondary anti-Cy2 and anti-Cy3 antibodies (EMD Millipore; 1 : 500) and CD1d and MOMA-1 with a biotinylated secondary antibody (DIANOVA Vertriebs-Gesellschaft mbH, Hamburg, Germany), treated with streptavidin-horseradish peroxidase and stained with tyramide (Cy3) and fluorescein (FITC). Nuclei were counterstained with Hoechst 33258 (Life Technologies GmbH, Darmstadt, Germany). Slices were mounted with Immuno Mount (Fisher Scientific GmbH, Schwerte, Germany) and analyzed on an Olympus BX51 (Olympus, Hamburg, Germany).

Transmission electron microscopy. Cells were pelleted, fixed in 2.5% glutaraldehyde, 2% PFA and 0.05% tannic acid and later treated with 2% osmium tetroxide. After staining with 1.5% uranylacetate and 1.5% phosphotungstic acid, pellets were embedded in epoxide resin (Spurr) and dissected in 70- to 80-nm-thick slices on an ultramicrotome (Reichert Ultracut; Reichert-Jung, Vienna, Austria). Images (30 KO and 32 WT) were taken on a Hitachi H 600 transmission electron microscope (Hitachi High Technologies America, Schaumburg, IL, USA).

Ca^{2+} measurements

Flow cytometry: Cells were incubated in culture medium consisting of RPMI 1640 (Fisher Scientific GmbH) supplemented with 10% FCS (Fisher Scientific GmbH), 100 U/ml penicillin and 100 μg/ml streptomycin (Invitrogen), 1% glutamax (Invitrogen) and 0.1% β-mercaptoethanol (Fisher Scientific GmbH), and the Ca^{2+} concentration was adjusted with 1M $CaCl_2$ and 1M EGTA. A total of 1×10^6 cells per ml were loaded with either 5 μM Fluo8-AM (Santa Cruz Biotechnology, Inc., Dallas, TX, USA), 2 μM Rhod2-AM (AAT Bioquest, Sunnyvale, CA, USA) or 5 μM CellROX (Fisher Scientific GmbH), washed, measured on a BD FACSCalibur or BD FACS Canto II (BD Bioscience) and analyzed with FlowJo, LLC. For pH-dependent measurements, cells were resuspended in HBSS (Fisher Scientific GmbH) adjusted to the indicated values with 1M HCl and 1M NaOH, directly after staining and measured immediately.

Ca^{2+} kinetics: Fura2 Ca^{2+} imaging experiments were conducted on a BD Pathway 855 High Content Imaging System (BD Bioscience). The 96-well imaging plates (BD Bioscience) were coated with 5 mg/ml BSA (Carl Roth) and 0.01% (w/v) poly-L-lysine (Sigma-Aldrich, St. Louis, MO, USA), splenocytes seeded at a density of 150 000 cells per well and loaded with 3 μM Fura2-AM (Life Technologies GmbH) in HBSS at RT for 20 min before the experiment. SOCE was quantified by a high-throughput method previously validated using STIM1 $-/-$ mouse embryonic fibroblasts and shown to be reliable.[40] Ratiometric Fura2-AM values were converted to absolute Ca^{2+} values as described[41] and analyzed with Attovision (BD Bioscience). For measuring the Ca^{2+} kinetics of B and T cells, splenocytes were incubated with 3 μM Fluo8 for 30 min at RT. Cells were washed once in DMEM without phenol red (Fisher Scientific GmbH) and resuspended at 40×10^6 cells per ml in the washing medium. A total of 2×10^6 cells were additionally incubated with 3 μg/ml biotinylated anti-CD3 antibody (Affymetrix eBioscience) for 10 min at RT, and before the measurement, 2×10^6 cells were transferred into 500 μl Ringer solution (Fresenius Kabi, Bad Homburg, Germany). After recording the baseline for 1 min in a FACS Canto II flow cytometer, either 3 μg/ml streptavidin (Fisher Scientific GmbH) were added to the cells, which were previously incubated with biotinylated anti-CD3 antibody or 10 μg/ml anti-IgM (Jackson ImmunoResearch Laboratories, Inc., West Grove, PA, USA). Data were recorded for 5 min and analyzed with the kinetics module of FlowJo, LLC.

Immunoblotting. Splenocytes were lysed in ice-cold CelLytic M buffer (Sigma-Aldrich) containing Mini Complete Protease Inhibitor Cocktail (Sigma-Aldrich) and centrifuged for 30 min at 16 000 × *g*. Subcellular fractionations were prepared as described previously.[42] Fifty micrograms of protein lysates were blotted and incubated with primary antibodies (diluted 1 : 1000) as follows: IP3R Pan (Rbt475),[43] ERp57 (Cell Signaling; no. 2881), Ero1-Lα (Cell Signaling; no. 3264), BIP (Cell Signaling; no. 3177), ERp72 (Cell Signaling; no. 5033), ERp44 (Cell Signaling; no. 3798), GrP94 (Cell Signaling; no. 2104), IκBα (Cell Signaling; no. 4814), phospho-IκBα (Cell Signaling; no. 2859), NF-κB p65 (Cell Signaling; no. 8242), phospho-NF-κB p65 (Cell Signaling; no. 3033), ubiquitin (Dako Deutschland GmbH, Hamburg, Germany; no. Z0458), STIM1 (stromal interaction molecule 1; Abnova (Taipei, Taiwan); no. h0000678-m01), ORAI1 (1 : 500; Alomone Labs, Jerusalem, Israel; no. ACC-062), NFATc1 (7A6) (1:200; Santa Cruz Biotechnology, Inc.; no. msc-7294), NF-κB2 p100/p52 (Cell Signaling; no. 4882), HDAC1 (Cell Signaling; no. 2062), $\alpha\beta$-tubulin (Cell Signaling; no. 2148), RelB (Santa Cruz Biotechnology, Inc.; no. sc-226), RelA (Santa Cruz Biotechnology, Inc.; no. sc-8008), c-Rel (Santa Cruz Biotechnology, Inc.; no. sc-71), NF-κB2 p105/p50 (Santa Cruz Biotechnology, Inc.; no. sc-7178), Serca2b (a kind gift from Frank Wuytack and Peter Vangheluwe), calreticulin (1 : 500), calnexin C20 (1 : 500), calnexin H70 (1 : 500), HSPA8 (Cell Signaling; no. 8444) and actin (1 : 4000; EMD Millipore; no. MAB1501). Antisera without vendor were obtained from the Bultynck Lab (Leuven, Belgium). Secondary antibodies used were as follows: anti-mouse or anti-rabbit IgG (Fc) infrared fluorescence conjugated secondary antibodies (LI-COR, Lincoln, NE, USA; 1 : 30 000). The membranes were scanned for infrared fluorescence at 680 and 800 nm using the Odyssey System (LI-COR) and the signal was analyzed with the image processing software ImageJ (National Institutes of Health, Bethesda, MD, USA).

Immunofluorescence staining and nuclear translocation assay. Splenocytes were seeded at a density of 150 000 cells per well on BSA and poly-L-lysine-coated 96-well imaging plates, fixed, blocked and incubated overnight with anti-NF-κB p65 (Cell Signaling; no. 8242) or anti-NFATc1 (Hybridoma Bank, Iowa City, IA, USA; no. 7A6) diluted 1 : 100 in blocking solution. After incubation with Cy3-labeled secondary antibody (EMD Millipore; 1 : 500) and nuclear staining with 150 nM DAPI (Sigma-Aldrich), pictures were taken on a Leica TSC SP5 confocal microscope (Leica Mikrosysteme Vertrieb GmbH) at x63 magnification and nuclear translocation of NF-κB p65 or NFATc1 was quantified in a BD Pathway 855 high content imaging system (BD Bioscience). Nuclear regions of interest were identified by DAPI signal and a concentric region around the nuclear region of interest was assessed as the cytoplasm. The ratio of the nuclear and cytoplasmic Cy3 signal was quantified with Attovision (BD Bioscience).

Measurement of mitochondrial oxygen consumption. A phosphorylation control protocol was performed for measurements of mitochondrial oxygen consumption of purified B cells using the high-resolution respirometer Oxygraph-2k (Oroboros Instruments Corp., Innsbruck, Austria). Intact B cells were monitored in two closed glass chambers under continuous stirring at 750 r.p.m. at 37 °C in 2 ml growth medium at a density of 3–4 × 10^6 cells per ml. After measurement of routine respiration, 2 μg/ml oligomycin was added to measure the leak respiration state. The electron transfer system capacity was determined by titration of the uncoupler carbonyl cyanide 4-(trifluoromethoxy) phenylhydrazone (FCCP) in 0.5 μM steps until a maximum flow was reached. Respiration was inhibited by application of 0.5 μM rotenone and 2.5 μM antimycin A to determine non-mitochondrial residual oxygen consumption (ROX). All substrates and inhibitors used were obtained from Sigma-Aldrich. Oxygen concentration and oxygen flow per cell were recorded in 2 s intervals using the DatLab Software 5.1 (Oroboros Instruments Corp.). To compare mitochondrial respiratory states, all values measured were corrected for ROX. All experiments were performed using instrumental background correction and after calibration of the polarographic oxygen sensors.

Viability and caspase assays. Splenocytes were magnetically sorted with an AutoMACS (magnetic cell seperation) cell separator (Miltenyi Biotec GmbH, Bergisch Gladbach, Germany), using either the CD43 (Ly-48) or Pan T-Cell Isolation Kit II (Miltenyi Biotec GmbH). Cell viability was assessed with LIVE/DEAD Fixable Dead Cell Stain Kit Green/Violet (Invitrogen). Caspase-3/7, -8 and -9 activity was measured with the Caspase Glo Assay Systems (Promega Corporation, Madison, WI, USA). In short, 50 000 B cells were seeded in 100 μl culture medium (as described above) in white-walled 96-well plates (Fisher Scientific GmbH). One hundred microliters of Caspase Glo reagent (Promega Corporation), containing the proteasome inhibitor MG-132, was added to the wells, the plate was shaken on a plate shaker for 1 min at 300 r.p.m. and then incubated for 40 min at RT. Luminescence was measured in a GENios Pro plate reader (Tecan Group AG, Männedorf, Switzerland).

XBP-1 splicing. PCR primers 5′-ACACGCTTGGGAATGGACAC-3′ and 5′-CCATGGGAAGATGTTCTGGG-3′ encompassing the spliced sequences in xbp-1 mRNA were used for PCR amplification with Platinum Taq Super Mix (Invitrogen). PCR products were separated on a 2.5% agarose gel (Sigma-Aldrich) and visualized with ethidium bromide (Sigma-Adrich). Band density was analyzed with the ImageJ software (National Institutes of Health) and was expressed as the density of spliced XBP-1 divided by the density of spliced XBP-1 plus unspliced XBP-1, where no splicing corresponds to 0%.

Active EAE and immunization. Female WT and KO mice were injected subcutaneously with 200 μg $MOG_{35–55}$ peptide (Biotrend Chemikalien GmbH, Köln, Germany) emulsified in Complete Freund's Adjuvant (1 : 1 (v/v)), which consisted of Incomplete Freund's Adjuvant supplemented with 5 mg/ml *Mycobacterium tuberculosis* H37RA (Difco Laboratories, Beckton, Dickinson, USA). For boosting, 200 ng Pertussis toxin (Sigma-Aldrich) was injected intraperitoneally on days 0 and 2 after immunization. From day 1, severity of the EAE was monitored and graded on a scale from 0 to 5: 0, no disease; 1, limp tail; 2, hind limb weakness; 3, hind limb paralysis; 4, hind and fore limb paralysis; 5, moribundity and death.

Immunoglobulin measurements. For immunizations, mice were injected intraperitoneally with 100 μg NPCG (Biosearch Technologies, Petaluma, CA, USA). Serum was collected from the peripheral blood and the immunoglobulin concentrations and NPCG-specific antibodies were determined by ELISA. For *in vitro* class switch experiments, splenocytes were cultured in triplicates of 300 000 treated with LPS (Sigma-Aldrich; 50 μg/ml)+IL4 (R&D Systems, Inc., Minneapolis, MN, USA; 20 ng/ml) for 4 days. The frequency of switched cells was measured by flow cytometry by gating on IgM^- $IgG1^+$ events. For each sample 200 000 events were acquired for analysis.

Statistical analysis. Data were analyzed as mean ± S.D., and the statistical significance was analyzed using two-tailed *t*-tests or analysis of variance (ANOVA) with Tukey's multiple comparison test as indicated.

Conflict of Interest

The authors declare no conflict of interest.

Acknowledgements. This work was supported by DFG ME1922/9-1 (to AM) and the Forschungskommission HHU (to AM and HHH).

Author contributions

DL, MG, AW, HHH, NH and AM designed the experiments with advice from GB, JBP and HdS. DL, TS, AG, PA, BK, MG, KZ, PAQ, MH and PA performed the experiments. DL, TS, BK, MG, KZ, NH and AM analyzed the data. DL, JCR and AM wrote the manuscript.

1. Berridge MJ, Bootman MD, Roderick HL. Calcium: calcium signalling: dynamics, homeostasis and remodelling. *Nat Rev Mol Cell Biol* 2003; **4**: 517–529.
2. Demaurex N, Distelhorst CW. Cell biology. Apoptosis – the calcium connection. *Science* 2003; **300**: 65–67.
3. Hetz C. The unfolded protein response: controlling cell fate decisions under ER stress and beyond. *Nat Rev Mol Cell Biol* 2012; **13**: 89–102.
4. Henke N, Lisak DA, Schneider L, Habicht J, Pergande M, Methner A. The ancient cell death suppressor BAX inhibitor-1. *Cell Calcium* 2011; **50**: 251–260.
5. Xu Q, Reed JC. Bax inhibitor-1, a mammalian apoptosis suppressor identified by functional screening in yeast. *Mol Cell* 1998; **1**: 337–346.
6. Chae H-J, Kim H-R, Xu C, Bailly-Maitre B, Krajewska M, Krajewski S *et al.* BI-1 regulates an apoptosis pathway linked to endoplasmic reticulum stress. *Mol Cell* 2004; **15**: 355–366.
7. Westphalen BC, Wessig J, Leypoldt F, Arnold S, Methner A. BI-1 protects cells from oxygen glucose deprivation by reducing the calcium content of the endoplasmic reticulum. *Cell Death Differ* 2005; **12**: 304–306.
8. Bultynck G, Kiviluoto S, Henke N, Ivanova H, Schneider L, Rybalchenko V *et al.* The C terminus of Bax inhibitor-1 forms a Ca^{2+}-permeable channel pore. *J Biol Chem* 2012; **287**: 2544–2557.
9. Lisak DA, Schacht T, Enders V, Habicht J, Kiviluoto S, Schneider J *et al.* The transmembrane Bax inhibitor motif (TMBIM) containing protein family: Tissue expression,

intracellular localization and effects on the ER CA(2+)-filling state. *Biochim Biophys Acta* 2015; **1853**: 2104–2114.
10. Kiviluoto S, Luyten T, Schneider L, Lisak D, Rojas-Rivera D, Welkenhuyzen K *et al.* Bax Inhibitor-1-mediated Ca(2+) leak is decreased by cytosolic acidosis. *Cell Calcium* 2013; **54**: 186–192.
11. Chang Y, Bruni R, Kloss B, Assur Z, Kloppmann E, Rost B *et al.* Structural basis for a pH-sensitive calcium leak across membranes. *Science* 2014; **344**: 1131–1135.
12. Bailly-Maitre B, Bard-Chapeau E, Luciano F, Droin N, Bruey J-M, Faustin B *et al.* Mice lacking bi-1 gene show accelerated liver regeneration. *Cancer Res* 2007; **67**: 1442–1450.
13. Bailly-Maitre B, Fondevila C, Kaldas F, Droin N, Luciano F, Ricci J-E *et al.* Cytoprotective gene bi-1 is required for intrinsic protection from endoplasmic reticulum stress and ischemia–reperfusion injury. *Proc Natl Acad Sci USA* 2006; **103**: 2809–2814.
14. Lisbona F, Rojas-Rivera D, Thielen P, Zamorano S, Todd D, Martinon F *et al.* BAX inhibitor-1 is a negative regulator of the ER stress sensor IRE1alpha. *Mol Cell* 2009; **33**: 679–691.
15. Kiviluoto S, Schneider L, Luyten T, Vervliet T, Missiaen L, De Smedt H *et al.* Bax inhibitor-1 is a novel IP_3 receptor-interacting and -sensitizing protein. *Cell Death Dis* 2012; **3**: e367.
16. Gilmore TD, Herscovitch M. Inhibitors of NF-kappaB signaling: 785 and counting. *Oncogene* 2006; **25**: 6887–6899.
17. Weih DS, Yilmaz ZB, Weih F. Essential role of RelB in germinal center and marginal zone formation and proper expression of homing chemokines. *J Immunol* 2001; **167**: 1909–1919.
18. Hövelmeyer N, Wunderlich FT, Massoumi R, Jakobsen CG, Song J, Wörns MA *et al.* Regulation of B cell homeostasis and activation by the tumor suppressor gene CYLD. *J Exp Med* 2007; **204**: 2615–2627.
19. Guo F, Weih D, Meier E, Weih F. Constitutive alternative NF-kappaB signaling promotes marginal zone B-cell development but disrupts the marginal sinus and induces HEV-like structures in the spleen. *Blood* 2007; **110**: 2381–2389.
20. Dolmetsch RE, Xu K, Lewis RS. Calcium oscillations increase the efficiency and specificity of gene expression. *Nature* 1998; **392**: 933–936.
21. Dolmetsch RE, Lewis RS, Goodnow CC, Healy JI. Differential activation of transcription factors induced by Ca^{2+} response amplitude and duration. *Nature* 1997; **386**: 855–858.
22. Pahl HL, Sester M, Burgert HG, Baeuerle PA. Activation of transcription factor NF-kappaB by the adenovirus E3/19K protein requires its ER retention. *J Cell Biol* 1996; **132**: 511–522.
23. Pahl HL, Baeuerle PA. A novel signal transduction pathway from the endoplasmic reticulum to the nucleus is mediated by transcription factor NF-kappa B. *EMBO J* 1995; **14**: 2580–2588.
24. Pahl HL, Baeuerle PA. Activation of NF-kappa B by ER stress requires both Ca^{2+} and reactive oxygen intermediates as messengers. *FEBS Lett* 1996; **392**: 129–136.
25. Davies SP, Reddy H, Caivano M, Cohen P. Specificity and mechanism of action of some commonly used protein kinase inhibitors. *Biochem J* 2000; **351**: 95–105.
26. Zhang SL, Yeromin AV, Zhang XH-F, Yu Y, Safrina O, Penna *et al.* Genome-wide RNAi screen of Ca(2+) influx identifies genes that regulate Ca(2+) release-activated Ca(2+) channel activity. *Proc Natl Acad Sci USA* 2006; **103**: 9357–9362.
27. Prakriya M, Feske S, Gwack Y, Srikanth S, Rao A, Hogan PG. Orai1 is an essential pore subunit of the CRAC channel. *Nature* 2006; **443**: 230–233.
28. White C, Li C, Yang J, Petrenko NB, Madesh M, Thompson CB *et al.* The endoplasmic reticulum gateway to apoptosis by Bcl-X(L) modulation of the InsP3R. *Nat Cell Biol* 2005; **7**: 1021–1028.
29. Li P, Nijhawan D, Budihardjo I, Srinivasula SM, Ahmad M, Alnemri ES *et al.* Cytochrome *c* and dATP-dependent formation of Apaf-1/caspase-9 complex initiates an apoptotic protease cascade. *Cell* 1997; **91**: 479–489.
30. Sano R, Hou Y-CC, Hedvat M, Correa RG, Shu C-W, Krajewska M *et al.* Endoplasmic reticulum protein BI-1 regulates Ca^{2+}-mediated bioenergetics to promote autophagy. *Genes Dev* 2012; **26**: 1041–1054.
31. Zhong F, Harr MW, Bultynck G, Monaco G, Parys JB, De Smedt H *et al.* Induction of Ca^{2+}-driven apoptosis in chronic lymphocytic leukemia cells by peptide-mediated disruption of Bcl-2-IP3 receptor interaction. *Blood* 2011; **117**: 2924–2934.
32. Smith KG, Light A, Nossal GJ, Tarlinton DM. The extent of affinity maturation differs between the memory and antibody-forming cell compartments in the primary immune response. *EMBO J* 1997; **16**: 2996–3006.
33. Suzuki J, Kanemaru K, Ishii K, Ohkura M, Okubo Y, Iino M. Imaging intraorganellar Ca^{2+} at subcellular resolution using CEPIA. *Nat Commun* 2014; **5**: 4153.
34. Favre CJ, Schrenzel J, Jacquet J, Lew DP, Krause KH. Highly supralinear feedback inhibition of Ca^{2+} uptake by the Ca^{2+} load of intracellular stores. *J Biol Chem* 1996; **271**: 14925–14930.
35. Mogami H, Tepikin AV, Petersen OH. Termination of cytosolic Ca^{2+} signals: Ca^{2+} reuptake into intracellular stores is regulated by the free Ca^{2+} concentration in the store lumen. *EMBO J* 1998; **17**: 435–442.
36. Li Y, Camacho P. Ca^{2+}-dependent redox modulation of SERCA 2b by ERp57. *J Cell Biol* 2004; **164**: 35–46.
37. Hetz C, Bernasconi P, Fisher J, Lee A-H, Bassik MC, Antonsson B *et al.* Proapoptotic BAX and BAK modulate the unfolded protein response by a direct interaction with IRE1alpha. *Science* 2006; **312**: 572–576.
38. Scorrano L, Oakes SA, Opferman JT, Cheng EH, Sorcinelli MD, Pozzan T *et al.* BAX and BAK regulation of endoplasmic reticulum Ca^{2+}: a control point for apoptosis. *Science* 2003; **300**: 135–139.
39. Oakes SA, Scorrano L, Opferman JT, Bassik MC, Nishino M, Pozzan T *et al.* Proapoptotic BAX and BAK regulate the type 1 inositol trisphosphate receptor and calcium leak from the endoplasmic reticulum. *Proc Natl Acad Sci USA* 2004; **102**: 105–110.
40. Henke N, Albrecht P, Pfeiffer A, Toutzaris D, Zanger K, Methner A. Stromal interaction molecule 1 (STIM1) is involved in the regulation of mitochondrial shape and bioenergetics and plays a role in oxidative stress. *J Biol Chem* 2012; **287**: 42042–42052.
41. Williams DA, Fay FS. Intracellular calibration of the fluorescent calcium indicator Fura-2. *Cell Calcium* 1990; **11**: 75–83.
42. Sasaki Y, Derudder E, Hobeika E, Pelanda R, Reth M, Rajewsky K *et al.* Canonical NF-kappaB activity, dispensable for B cell development, replaces BAFF-receptor signals and promotes B cell proliferation upon activation. *Immunity* 2006; **24**: 729–739.
43. Bultynck G, Szlufcik K, Kasri NN, Assefa Z, Callewaert G, Missiaen L *et al.* Thimerosal stimulates Ca^{2+} flux through inositol 1,4,5-trisphosphate receptor type 1, but not type 3, via modulation of an isoform-specific Ca^{2+}-dependent intramolecular interaction. *Biochem J* 2004; **381**: 87–96.

Supplementary Information accompanies this paper on Cell Death and Differentiation website (http://www.nature.com/cdd)